JACS Au
AN OPEN ACCESS JOURNAL OF THE AMERICAN CHEMICAL SOCIETY

Editors' Choice
Open Access

pubs.acs.org/jacsau
Article

Multiple Dissociation Pathways in HNCO Decomposition Governed by Potential Energy Surface Topography

Zhiguo Zhang,[#] Hao Wu,[#] Zhichao Chen,* Yanlin Fu, Bina Fu,* Dong H. Zhang, Xueming Yang, and Kaijun Yuan*

Cite This: *JACS Au* 2023, 3, 2855−2861
Read Online

ACCESS | Metrics & More | Article Recommendations | Supporting Information

ABSTRACT: The exquisite features of molecular photochemistry are key to any complete understanding of the chemical processes governed by potential energy surfaces (PESs). It is well established that multiple dissociation pathways relate to nonadiabatic transitions between multiple coupled PESs. However, little detail is known about how the single PES determines reaction outcomes. Here we perform detailed experiments on HNCO photodissociation, acquiring the state-specific correlations of the NH ($a^1\Delta$) and CO ($X^1\Sigma^+$) products. The experiments reveal a trimodal CO rotational distribution. Dynamics simulations based on a full-dimensional machine-learning-based PES of HNCO unveil three dissociation pathways exclusively occurring on the S_1 excited electronic state. One pathway, following the minimum energy path (MEP) via the transition state, contributes to mild rotational excitation in CO, while the other two pathways deviating substantially from the MEP account for relatively cold and hot CO rotational state populations. These peculiar dynamics are unambiguously governed by the S_1 state PES topography, i.e., a narrow acceptance cone in the vicinity of the transition state region. The dynamical picture shown in this work will serve as a textbook example illustrating the importance of the PES topography in molecular photochemistry.

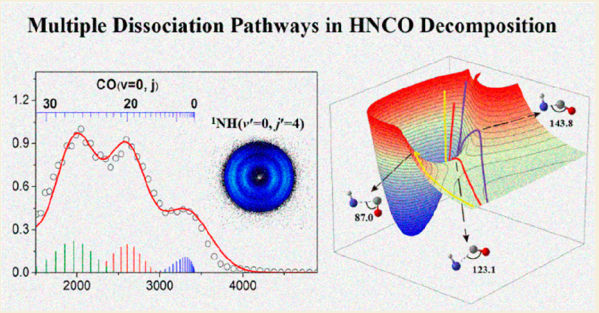

KEYWORDS: *State-resolved photodissociation, multiple dissociation pathways, potential energy surface, excited states, quasi-classical dynamics*

INTRODUCTION

Multiple dissociation pathways (MDPs) are ubiquitous in photochemistry when electronically excited states are involved. The interpretation of such experimental phenomena is usually related to dynamics governed by multiple coupled potential energy surfaces (PESs).[1−3] In the past decades, a rich gamut of nonadiabatic dynamics, for instance, passage through conical intersections,[4,5] Coriolis couplings,[6,7] and vibronic couplings,[8,9] have been identified from MDPs in molecular photochemistry. MDPs may also take place in a single electronic state and are governed by the topography of PES. However, few examples have hitherto been identified in photochemistry studies. Therefore, little detail is known about how the electronic state of the PES determines MDPs. Here we demonstrate the MDPs in HNCO decomposition, which occur solely in a single electronically excited state.

HNCO photodissociation has attracted much attention since its important role in energetic materials combustion[10,11] and in interstellar space.[12−14] It also serves as a benchmark system for understanding MDPs in polyatomic molecular photochemistry. Excitation to the HNCO first excited singlet state, $S_1(^1A'')$, which spans the wavelength range $180 < \lambda < 280$ nm,[15−17] leads to three fragment channels via various dissociation pathways such as internal conversion (IC), intersystem crossing (ISC), and direct dissociation processes:[18]

$$\mathrm{HNCO}(S_1) \rightarrow \mathrm{NH}(X^3\Sigma^-) + \mathrm{CO}(X^1\Sigma^+) \quad D_0 = 30060 \pm 30\ \mathrm{cm}^{-1} \tag{1}$$

$$\mathrm{H}(^2S) + \mathrm{NCO}(X^2\Pi) \quad D_0 = 38370 \pm 30\ \mathrm{cm}^{-1} \tag{2}$$

$$\mathrm{NH}(a^1\Delta) + \mathrm{CO}(X^1\Sigma^+) \quad D_0 = 42750 \pm 30\ \mathrm{cm}^{-1} \tag{3}$$

The S_1 electronic state correlates adiabatically with channels 2 and 3. However, due to a large barrier of ~8700 cm^{-1} in the H + NCO dissociation channel, direct dissociation on the S_1 state to yield channel 2 is not possible without a sufficiently high excitation energy.[19−22] Thus, for energies below the threshold of channel 3, HNCO molecules dissociate on the $S_0(^1A')$

Received: July 27, 2023
Revised: August 24, 2023
Accepted: August 31, 2023
Published: September 23, 2023

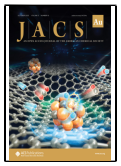

https://doi.org/10.1021/jacsau.3c00414
JACS Au 2023, 3, 2855−2861

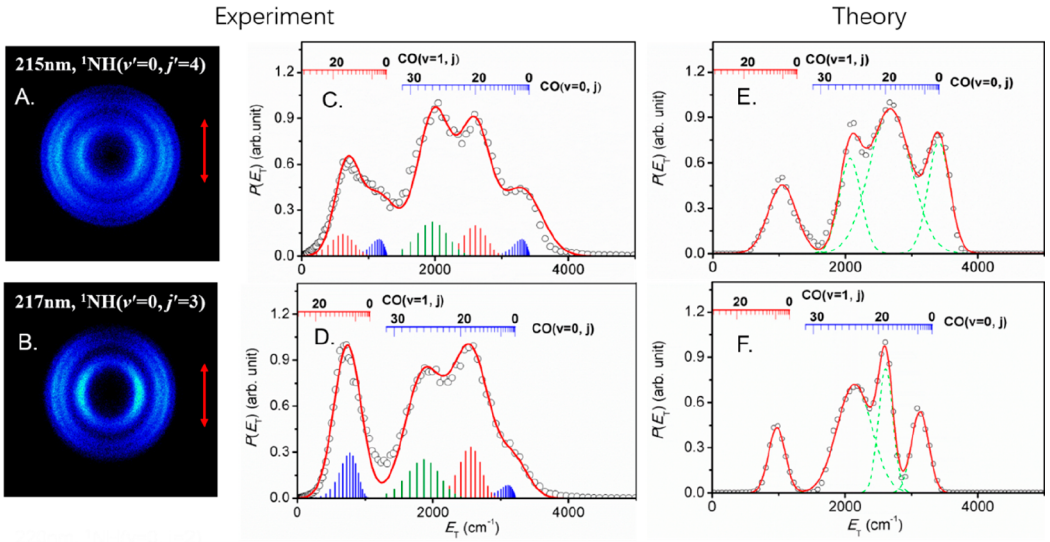

Figure 1. Time-sliced velocity map images of (A) ^{1}NH ($v' = 0, j' = 4$) products from photodissociation of HNCO at 215 nm and (B) ^{1}NH ($v' = 0, j' = 3$) products from photodissociation of HNCO at 217 nm. The double red arrow indicates the polarization direction of the dissociation laser. $P(E_T)$ spectra of (C) ^{1}NH ($v' = 0, j' = 4$) at 215 nm and (D) ^{1}NH ($v' = 0, j' = 3$) at 217 nm photolysis, derived from those images, are shown in black empty circles, along with the best-fit simulation of the spectra, in red. The superposed combs in C) and D) indicate the E_T values associated with formation of the various CO ($v = 0$ and 1, j). The stick spectra in blue, red, and green shown underneath the experimental curves are three model Gaussian j distributions returned by fitting. $P(E_T)$ spectra of (E) ^{1}NH ($v' = 0, j' = 4$) at 215 nm and (F) ^{1}NH ($v' = 0, j' = 3$) at 217 nm photolysis returned by theoretical calculations, shown in black empty circles, and each rotational distribution is fitted by green dashed lines. Both experimental and theoretical results show trimodal rotational distributions of CO ($v = 0$) products.

ground state following IC from S_1 to S_0, leading to the fragment channel 2;[23−27] or further undergo ISC from S_0 to the triple state $T_1(^3A'')$ and dissociate on T_1 state to form channel 1.[28−32] On the other hand, there is a low barrier of ∼470 cm^{-1} for channel 3, direct dissociation on the S_1 state PES quickly dominates after excitation energies exceeding this small barrier, yielding electronically excited NH ($a^1\Delta$) fragment and CO ($X^1\Sigma^+$).[33−35] For simplicity, NH ($a^1\Delta$) is denoted by ^{1}NH.

In the past years, channel 3 has been investigated at wavelengths between 193 and 230 nm.[36−39] A cold ^{1}NH rotational distribution together with a hot CO distribution was identified. By using the high resolution velocity map ion (VMI) imaging technique, Zhang et al.[40,41] reported the pair-correlation between ^{1}NH and CO products at 201 nm photolysis. A bimodal rotational distribution was observed in the CO product, which was explained as resulting from the involvement of two HNCO isomers (cis and trans) in the dissociation process. Such mechanism was questioned by recent theoretical calculations.[42] Bonnet et al.[42] reproduced the bimodality of CO based on an approximated six-dimensional S_1 state PES of HNCO, and attributed the CO bimodal distribution to be an impulsive-deflective mechanism due to two repulsive walls of the S_1 state PES. Similar bimodality has also been reported in CO_2[43] and NO_2[44] photodissociation, but the underlying dynamics are still elusive. The product multimodal distributions are centrally important as they often indicate the presence of MDPs, and unraveling the multimodality is key to understanding the complicated features of molecular photochemistry.

In this Article, we investigate channel 3 from HNCO photodissociation at 215 and 217 nm and determine the state-specific correlations of the ^{1}NH and CO products. The experimental results display previously undetected trimodal CO rotational distributions. Theoretical calculations based on a new accurate full-dimensional neural network PES of the S_1 electronic state demonstrate that this intriguing feature arises from three distinct dissociation pathways, comprising one pathway along the minimum energy path (MEP) via the transition state as well as two additional pathways substantially deviating from MEP. These characteristics and pathways are unambiguously governed by the topography of the S_1 potential energy landscape, which exhibits a narrow bottleneck in the vicinity of the transition state region.

RESULTS AND DISCUSSION

The experiments were performed using a time-sliced VMI apparatus, which has been described previously.[45−47] Briefly, HNCO in a molecular beam was excited to the S_1 electronic state by absorbing one photon of 215 or 217 nm. The nascent ^{1}NH photofragments were then state-selectively ionized using (2 + 1) resonance enhanced multiphoton ionization (REMPI). Postionization, the ^{1}NH products were detected by the VMI detector (see Methods section for more detail).

Figure 1A and B shows typical raw images of ^{1}NH ($v' = 0$) products in specific rotational levels recorded following the photolysis of HNCO at 215 and 217 nm, respectively. The images were recorded by accumulating the REMPI ^{1}NH$^+$ signals over 40000 laser shots with background subtraction. Additional images, taken from ^{1}NH ($v' = 0, j' = 2−5$) at 215 nm and NH ($v' = 0, j' = 2−4$) at 217 nm, are displayed in Figures S1 and S2 of the Supporting Information (SI). The double headed arrow in Figure 1 shows the direction of the polarization vector of the photolysis laser. All observed images are pump−probe- and molecular beam dependent. Well-resolved, concentric rings with different intensities can be clearly observed in the displayed images. These structures can be readily assigned to population of different rovibrational states of the partner CO product in the ^{1}NH + CO dissociation process, channel 3.

https://doi.org/10.1021/jacsau.3c00414
JACS Au 2023, 3, 2855−2861

The radii of the ring structures in the VMI images can be used to determine the velocity distribution of the ^{1}NH products. These velocities can then be converted to a total kinetic energy release $P(E_T)$ spectrum of the ^{1}NH + CO products using linear momentum conservation arguments. Figure 1C and D displays $P(E_T)$ spectra obtained by integrating signals over all angles in the respective images. The internal energy distributions of the CO coproduct can then be obtained from the corresponding $P(E_T)$ spectrum using the law of energy conservation. The energy combs representing the rovibrational states of CO products are labeled in Figure 1C and D. As can be seen, the CO products can only be distributed in the lowest two vibrational states (v = 0 and 1). As the rotational excitation of the ^{1}NH (v' = 0) increases, the relative population of the correlated CO products in v = 1 decreases, implying the vibrational excitation of the CO product is anticorrelated to the ^{1}NH (v' = 0) rotational excitation (Figure S3). The CO product has a slightly higher vibrational excitation at 215 nm than that at 217 nm photolysis, due to the higher available energy at 215 nm.

In this work, the most interesting feature is that the CO (v = 0) rotational distributions display three partially resolved broad peaks, and such phenomena can all be observed in $P(E_T)$ spectra from ^{1}NH (v' = 0, j' = 2−5) at 215 nm and from NH (v' = 0, j' = 2−4) at 217 nm (Figures 1C, D and Figures S1 and S2), differs from previously observed at 201 nm[41] and 210 nm[38] HNCO photolysis. Although there is insufficient experimental resolution to resolve an individual j state, the structure in the $P(E_T)$ spectra must reflect solely the population distribution in the CO rotational states. The stick spectra in blue, red, and green shown underneath the experimental curves are three model Gaussian j distributions, which represent different j(CO) components, peaking at low-j ($j \approx 0-15$), middle-j ($j \approx 14-26$), and high-j ($j \approx 24-32$). Each stick spectrum was convolved with inherent instrumental resolution and the ^{1}NH recoil from the ionization step. The Gaussian fitting parameters were varied until the best fit to the experimental data was obtained. Three Gaussian functions provided a better fit to experiment than any other model distributions. The CO (v = 1) products at 215 nm photolysis demonstrate low-j and middle-j components except a high-j component, while at 217 nm photolysis the CO (v = 1) fragments only display a low-j component, which could be due to less available energy.

Previous studies[18−32] have demonstrated MDPs in HNCO decomposition from the initially excited S_1 electronic state, namely IC from S_1 to S_0 and dissociation in the S_0 state, IC from S_1 to S_0 followed by ISC from S_0 to T_1 and dissociation in the T_1 state, and direct dissociation in the S_1 state. At 215 and 217 nm, the excitation energies already exceed the small barrier in the S_1 state to form channel 3, therefore direct dissociation on this surface should dominate. From the anisotropic images shown in Figure 1A and B, the angular distributions of the ^{1}NH + CO channel were obtained by integrating the images over the relevant radius region. The corresponding product anisotropy parameters determined by fitting the angular distributions are shown in Figure S4. As can be seen, the anisotropy parameters of the ^{1}NH (v'=0, j') + CO (v = 0) are around −0.6 at 215 nm and about −0.7 at 217 nm. With j' increasing, the angular distribution becomes slightly less anisotropic, which can be explained by a nonaxial recoil impact model.[48] Nevertheless, the relatively large negative anisotropy parameters confirm the direct dissociation process for the N−C bond cleavage to channel 3 on the S_1 state. Thus, the trimodal CO rotational distributions observed in this work suggest the direct dissociation pathway on the S_1 state is itself trimodal. Such MDPs should be governed only by the PES topography of the S_1 state.

To characterize the detailed dissociation mechanism of HNCO photolysis in the S_1 state, we constructed a new, accurate full-dimensional S_1 state PES of HNCO using the neural network (NN) approach. The schematic of the S_1 state PES shown in Figure S5 gives details of *trans*-minimum (S1TM) and *cis*-minimum (S1CM) as well as associated transition states and product channels. The quasi-classical trajectory (QCT) dynamics calculations were performed based on the full-dimensional PES, with the initial condition sampled and final conditions analyzed in a quantum spirit. The theoretical results accurately reproduce the trimodal structure observed in the rotational distribution of CO (v = 0), as illustrated in Figure 1E and F. Further analysis demonstrates that this intriguing feature arises from three distinct reaction pathways determined by the potential energy topography of the S_1 state. Figure 2 displays the S_1 state PES of HNCO as a function of the dissociating N−C distance (r_{NC}) and the NCO enclosed angle (α), along with three representative trajectories projected onto the PES. It is evident that one reaction pathway follows the minimum energy path (MEP) via the transition state (S1TT3 shown in Figures S5 and S6) connecting the *trans*-minimum and products, resulting in a mild change in the

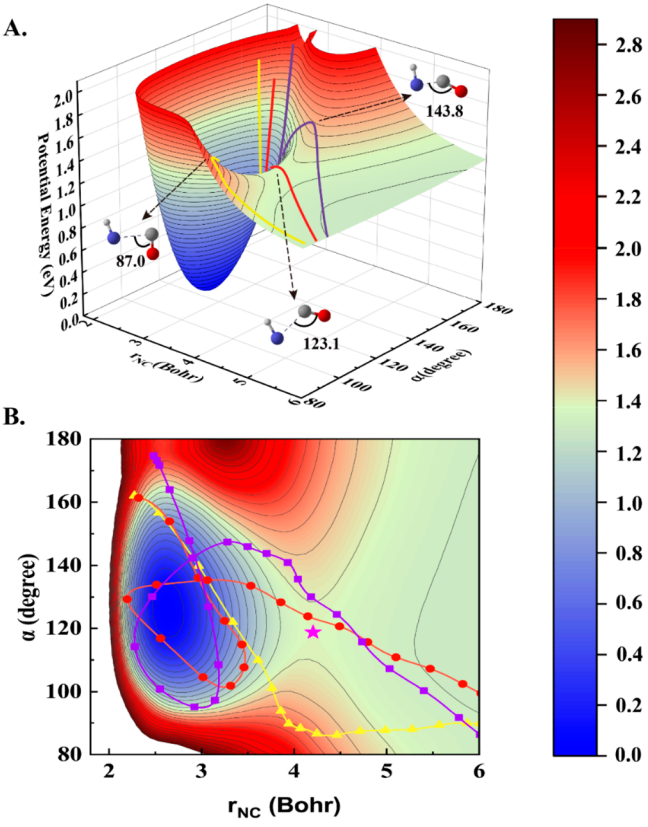

Figure 2. (A) Projections of three typical trajectories on the S_1 state PES as functions of N−C distance (r_{NC}) and NCO enclosed angle (α), with the rest of the degrees of freedom fully optimized. (B) Same as (A), except for the 2D contour plots of the PES. The transition state connecting the *trans*-minimum to the HN + CO products is indicated by the star symbol.

https://doi.org/10.1021/jacsau.3c00414
JACS Au 2023, 3, 2855−2861

NCO angle along the dissociating coordinate and consequently a moderate peak in the rotational state distribution. The exit angle, which corresponds to the NCO enclosed angle at the transition state (r_{NC} = 4.2 bohr) for this pathway, measures approximately 120°. However, as depicted in Figure 2, this pathway originating from the *trans*-minimum via the transition state is narrow, exhibiting a small acceptance cone. Consequently, many trajectories become frustrated along this decomposition route, but deviate from the MEP. The MEP is flanked by two potential walls or ridges. One wall features a larger exit angle (~140°) compared to the transition state, while the other wall exhibits a smaller exit angle (~90°). These differences in exit angles have a significant impact on the final outcomes. The trajectory indicated by the yellow curve experiences strong deflection from the lower potential wall, finally becoming nearly parallel to the *x*-axis with minimal variation in the NCO angle. With an exit angle close to 90°, this pathway results in the direct ejection of the CO molecule with a high radial velocity but limited angular velocity (∠NCO), ultimately leading to a rotationally cold product. On the other hand, the trajectory depicted by the blue curve undergoes deflection from the upper potential wall. This deflection primarily occurs in the radial direction at larger exit angles, leading to a decrease in the radial velocity along r_{NC} and an increase in the angular velocity. Consequently, this pathway yields a rotationally hot CO product. The distribution of exit angles (NCO angle at r_{NC} = 4.2 bohr) for all reactive trajectories, as shown in Figure 3, also exhibits a trimodal

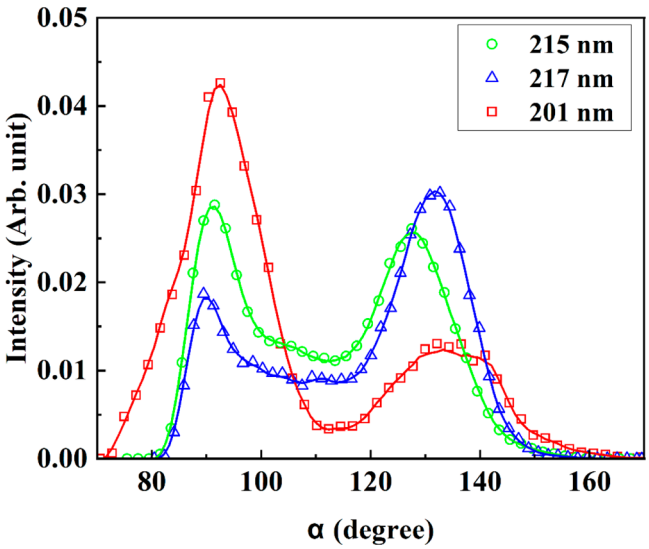

Figure 3. Computed overall distributions of the exit angles for ^{1}NH ($v' = 0, j' = 4$) products at the photolysis energy of 215 nm and ^{1}NH ($v' = 0, j' = 3$) products at 217 nm, together with ^{1}NH ($v' = 0, j' = 2$) products at a higher photolysis energy of 201 nm. The product CO is in vibrationally ground state with all the accessible rotational states.

structure at 215 and 217 nm excitation, further confirming our findings regarding the three reaction pathways dictated by the potential energy landscape. We anticipate that quantum interference between these three pathways also plays a crucial role in generating the distinct triple peaks observed in the kinetic energy distribution of CO ($v = 0$).[49,50]

In contrast, fewer trajectories follow the MEP at a higher photoexcitation energy of 201 nm, leading to the absence of the middle-*j* CO ($v = 0$) peak. As can be seen in Figure 3, the distribution of exit angles for the reactive trajectories around 120° at 201 nm is also substantially lower than that at 215 and 217 nm, in consistent with the bimodal feature of kinetic energy spectra observed in experiments at 201 nm.[41] It is worth noting that the current theory based on the full-dimensional NN PES exhibits obviously improved agreement with the experimental results at 201 nm (Figure S7), compared with the previous works.[42] This outcome underscores the significance of attaining high accuracy in the PES for the accurate characterization of mechanisms and reproduction of experimental observations.

CONCLUSIONS

In summary, detailed correlated product state distributions of CO (v) and ^{1}NH (v'=0, j') from HNCO photodissociation have been measured using the time-sliced velocity-mapped ion imaging technique. The results display that the CO ($v = 0$) products arising from the direct dissociation pathway on the S_1 state PES have a trimodal rotational state distribution. The measurements and associated QCT calculations provide additional insights into this prototypical unimolecular reaction: three distinct dissociation pathways occur in the S_1 state, involving one pathway along the MEP via the transition state as well as two additional pathways substantially deviating from MEP. These subtle effects are entirely governed by the topography of the S_1 potential energy landscape, demonstrating additional complexity in molecular photochemistry. We believe that such a peculiar dynamical feature could be general in unimolecular reaction, which provides the most rigorous test of the quality of PES and theoretical methods.

METHODS

HNCO photodissociation at 215 and 217 nm was investigated using a sliced velocity map ion imaging setup, which has been described previously.[41,51−54] In brief, a pulsed molecular beam was produced by expanding 2% HNCO in argon at total pressures of ~1 bar. The mixtures were expanded into the source chamber through a 0.5 mm diameter pulsed nozzle. The molecular beam was differentially pumped and collimated with a 1.5 mm diameter skimmer. About 38 mm downstream from the skimmer, the HNCO beam passed through a 2 mm pinhole in the first electrode plate and then was perpendicularly intersected with the photolysis laser beam.

The photolysis laser was generated by doubling the output of a tunable dye laser, which was pumped by the second harmonic of a Nd^{3+}:yttrium aluminum garnet (YAG) laser. In order to avoid multiphoton processes, < 0.5 mJ/pulse of the photolysis laser beam was used and focused onto the HNCO beam with a lens of 300 mm focal length. The ^{1}NH photofragment was then detected about 20 ns later by a focused probe laser beam generated by doubling the output of another tunable dye laser, which is pumped by the third harmonic of a second Nd:YAG laser. About 0.8 mJ/pulse of the probe laser was focused into the photodissociation region by using a 200 mm focal length lens. The ^{1}NH fragments were ionized by the $g^1\Delta(3p\pi) \leftarrow\leftarrow a^1\Delta$ (2 + 1) REMPI scheme, ~265 nm for ^{1}NH($v' = 0, j'$).[55] The two laser beams were counter propagated and spatially overlapped at the middle position of the HNCO beam between the third and the fourth electrode plates. The polarization direction of the photolysis laser was parallel to the detector plane, while that of the probe laser was perpendicular to the detector plane.

The $^1NH^+$ ions were accelerated by the focusing electric fields before hitting an imaging detector with dual 40 mm diameter Chevron multichannel plates (MCP) coupled to a phosphor screen (P47). The transient ion images on the phosphor screen were recorded by a cooled charge-coupled device (CCD) camera (ImagerPro2M 640 × 480 pixels, LaVision) and transferred to a computer on an every shot basis for event counting and data analysis.

https://doi.org/10.1021/jacsau.3c00414
JACS Au 2023, 3, 2855−2861

The final images are accumulated over 20000 laser shots or more, depending on the signal-to-noise ratio. Background signals were also acquired and subtracted from these images.

Theoretically, we constructed a new, accurate full-dimensional S_1 state PES of HNCO using the neural network (NN) approach[56−59] based on a data set consisting of 82202 (MRCI+Q)/aug-cc-pVTZ energy points. The dynamical propagation was basically based on the quantum trajectory (QCT), but with the initial condition sampled and final conditions analyzed in a quantum spirit. Those trajectories were initiated on S_1 with coordinates and momenta sampled from a Wigner distribution[60,61] characterizing the zero-point phase space of HNCO(S_0) and approximating the vertical excitation of a vibrational ground state wave packet. The trajectories were further propagated on S_1 using the velocity Verlet method until they reached the ^{1}NH + CO or H + NCO product channel. The Gaussian binning (GB) approach[62] was employed to analyze the final conditions, including the pair-correlated product kinetic energy distributions and vibrational state and rotational state distributions of ^{1}NH and CO. The Bohr quantization rule was applied to obtain the vibrational quantum numbers of products.[63]

■ ASSOCIATED CONTENT

Supporting Information

The Supporting Information is available free of charge at https://pubs.acs.org/doi/10.1021/jacsau.3c00414.

Detailed experimental and theoretical methods; supplementary figures; references (PDF)

■ AUTHOR INFORMATION

Corresponding Authors

Kaijun Yuan − *State Key Laboratory of Molecular Reaction Dynamics and Dalian Coherent Light Source, Dalian Institute of Chemical Physics, Chinese Academy of Sciences, Dalian 116023, China; University of Chinese Academy of Sciences, Beijing 100049, P. R. China; Hefei National Laboratory, Hefei 230088, China;* orcid.org/0000-0002-5108-8984; Email: kjyuan@dicp.ac.cn

Bina Fu − *State Key Laboratory of Molecular Reaction Dynamics and Dalian Coherent Light Source, Dalian Institute of Chemical Physics, Chinese Academy of Sciences, Dalian 116023, China; University of Chinese Academy of Sciences, Beijing 100049, P. R. China; Hefei National Laboratory, Hefei 230088, China;* orcid.org/0000-0003-1568-0259; Email: bina@dicp.ac.cn

Zhichao Chen − *State Key Laboratory of Molecular Reaction Dynamics and Dalian Coherent Light Source, Dalian Institute of Chemical Physics, Chinese Academy of Sciences, Dalian 116023, China*; Email: czc@dicp.ac.cn

Authors

Zhiguo Zhang − *State Key Laboratory of Molecular Reaction Dynamics and Dalian Coherent Light Source, Dalian Institute of Chemical Physics, Chinese Academy of Sciences, Dalian 116023, China; Key Laboratory of Functional Materials and Devices for Informatics of Anhui Educational Institutions and School of Physics and Electronic Engineering, Fuyang Normal University, Fuyang, Anhui 236041, China*

Hao Wu − *State Key Laboratory of Molecular Reaction Dynamics and Dalian Coherent Light Source, Dalian Institute of Chemical Physics, Chinese Academy of Sciences, Dalian 116023, China; University of Chinese Academy of Sciences, Beijing 100049, P. R. China*

Yanlin Fu − *State Key Laboratory of Molecular Reaction Dynamics and Dalian Coherent Light Source, Dalian Institute of Chemical Physics, Chinese Academy of Sciences, Dalian 116023, China*

Dong H. Zhang − *State Key Laboratory of Molecular Reaction Dynamics and Dalian Coherent Light Source, Dalian Institute of Chemical Physics, Chinese Academy of Sciences, Dalian 116023, China; University of Chinese Academy of Sciences, Beijing 100049, P. R. China; Hefei National Laboratory, Hefei 230088, China;* orcid.org/0000-0001-9426-8822

Xueming Yang − *State Key Laboratory of Molecular Reaction Dynamics and Dalian Coherent Light Source, Dalian Institute of Chemical Physics, Chinese Academy of Sciences, Dalian 116023, China; University of Chinese Academy of Sciences, Beijing 100049, P. R. China; Hefei National Laboratory, Hefei 230088, China; Department of Chemistry and Center for Advanced Light Source Research, College of Science, Southern University of Science and Technology, Shenzhen 518055, China;* orcid.org/0000-0001-6684-9187

Complete contact information is available at: https://pubs.acs.org/10.1021/jacsau.3c00414

Author Contributions

#Z.G.Z. and H.W. contributed equally. K.J.Y. and C.Z.C. designed the experiments. Z.G.Z. and C.Z.C. performed the experiments. K.J.Y. and X.M.Y. analyzed the data. H.W., Y.L.F., B.N.F., and D.H.Z. performed the theoretical calculation. Z.G.Z., K.J.Y. and B.N.F. prepared the manuscript. CRediT: Zhiguo Zhang investigation, writing-original draft; Hao Wu investigation, writing-original draft; Zhichao Chen investigation, supervision; Yanlin Fu investigation; Bina Fu methodology, funding acquisition, supervision, writing-original draft, writing-review & editing; Dong H. Zhang funding acquisition; Yang Xueming funding acquisition; Kaijun Yuan methodology, funding acquisition, supervision, writing-original draft, writing-review & editing. CRediT: **Zhiguo Zhang** investigation, writing-original draft.

Notes

The authors declare no competing financial interest.

■ ACKNOWLEDGMENTS

The experimental work was supported by the National Natural Science Foundation of China (Grant Nos. 22241304, 22225303, 22203093), the National Natural Science Foundation of China (NSFC Center for Chemical Dynamics (Grant No. 22288201)), the Scientific Instrument Developing Project of the Chinese Academy of Sciences (Grant No. GJJSTD20220001), the Innovation Program for Quantum Science and Technology (2021ZD0303304), the Innovation Fund Project of Dalian Institute of Chemical Physics (DICP I202112) and the Open Foundation of State Key Laboratory (Grant No. SKLMRD-K202313). The theoretical work was supported by the National Natural Science Foundation of China (Grant Nos. 22173099, 22203092), the Innovation Program for Quantum Science and Technology (2021ZD0303305) and the Dalian Innovation Support Program (Grant No. 2021RD05). X. Yang also thanks the Guangdong Science and Technology Program (Grant Nos. 2019ZT08L455 and 2019JC01 × 091), and the Shenzhen Science and Technology Program (Grant No. ZDSYS20200421111001787). Z. G. Zhang thanks the Natural

Science Research Project of Education Department of Anhui Province (No. 2023AH050426).

REFERENCES

(1) Yuan, K. J.; Dixon, R. N.; Yang, X. M. Photochemistry of the Water Molecule: Adiabatic versus Nonadiabatic Dynamics. *Acc. Chem. Res.* **2011**, *44*, 369−378.

(2) Hu, X. X.; Zhou, L. S.; Xie, D. Q. State-to-state Photodissociation Dynamics of the Water Molecule. *Wires Comput. Mol. Sci.* **2018**, *8*, 1350.

(3) Ashfold, M. N. R.; King, G. A.; Murdock, D.; Nix, M. G.; Oliver, T. A. A.; Sage, A. G. $\pi\sigma^*$ Excited States in Molecular Photochemistry. *Phys. Chem. Chem. Phys.* **2010**, *12*, 1218−1238.

(4) Dixon, R. N.; Hwang, D. W.; Yang, X. F.; Harich, S.; Lin, J. J.; Yang, X. Chemical "Double Slits": Dynamical Interference of Photodissociation Pathways in Water. *Science.* **1999**, *285*, 1249−1253.

(5) Chang, Y.; Yu, Y.; Wang, H. L.; Hu, X. X.; Li, Q. M.; Yang, J. Y.; Su, S.; He, Z. G.; Chen, Z. C.; Che, L.; Wang, X.; Zhang, W. Q.; Wu, G. R.; Xie, D. Q.; Ashfold, M. N. R.; Yuan, K. J.; Yang, X. M. Hydroxyl Super Rotors from Vacuum Ultraviolet Photodissociation of Water. *Nat. Commun.* **2019**, *10*, 1250.

(6) Zhao, Y.; Luo, Z.; Chang, Y.; Wu, Y.; Zhang, S.; Li, Z.; Ding, H.; Wu, G. J.; Campbell, S.; Hansen, C. S.; Crane, S. W.; Western, C. M.; Ashfold, M. N. R.; Yuan, K.; Yang, X. Rotational and Nuclear-spin Level Dependent Photodissociation Dynamics of H_2S. *Nat. Commun.* **2021**, *12*, 4459.

(7) Yuan, K. J.; Cheng, Y.; Cheng, L.; Guo, Q.; Dai, D.; Wang, X.; Yang, X. M.; Dixon, R. N. Nonadiabatic Dissociation Dynamics in H_2O: Competition between Rotationally and Nonrotationally Mediated Pathways. *Proc. Natl. Acad. Sci. U.S.A.* **2008**, *105*, 19148−19153.

(8) Dixon, R. N.; Oliver, T. A. A.; Cheng, L.; Cheng, Y.; Yuan, K. J.; Yang, X. M. Vibronically Induced Decay Paths from the $\tilde{C}\ ^1B_1$-state of Water and Its Isotopomers. *J. Chem. Phys.* **2013**, *138*, 104306.

(9) Zhao, Y.; Chen, J.; Luo, Z.; Chang, Y.; Yang, J.; Zhang, W.; Wu, G.; Crane, S. W.; Hansen, C. S.; Ding, H.; An, F.; Hu, X.; Xie, D.; Ashfold, M. N. R.; Yuan, K.; Yang, X. The Vibronic State Dependent Predissociation of H_2S: Determination of All Fragmentation Processes. *Chem. Sci.* **2023**, *14*, 2501−2517.

(10) Miller, J. A.; Bowman, C. T. Kinetic Modeling of the Reduction of Nitric Oxide in Combustion Products by Isocyanic Acid. *Int. J. Chem. Kinet.* **1991**, *23*, 289−313.

(11) Perry, R. A.; Siebers, D. L. Rapid Reduction of Nitrogen Oxides in Exhaust Gas Streams. *Nature.* **1986**, *324*, 657−658.

(12) Snyder, L. E.; Buhl, D. Interstellar Isocyanic Acid. *Astrophys. J.* **1972**, *177*, 619−623.

(13) Marcelino, N.; Brünken, S.; Cernicharo, J.; Quan, D.; Roueff, E.; Herbst, E.; Thaddeus, P. The Puzzling Behavior of HNCO Isomers in Molecular Clouds. *Astron. Astrophys.* **2010**, *516*, A105−A112.

(14) Nguyen-Q-Rieu; Henkel, C.; Jackson, J. M.; Mauersberger, R. Detection of HNCO in External Galaxies. *Astron. Astrophys.* **1991**, *241*, L33−L36.

(15) Dixon, R. N.; Kirby, G. H. Ultraviolet Absorption Spectrum of Isocyanic Acid. *Trans. Faraday Soc.* **1968**, *64*, 2002−2012.

(16) Rabalais, J. W.; McDonald, J. R.; McGlynn, S. P. Electronic States of HNCO, Cyanate Salts, and Organic Isocyanates. II. Absorption Studies. *J. Chem. Phys.* **1969**, *51*, 5103−5111.

(17) Rabalais, J. W.; McDonald, J. M.; Scherr, V.; McGlynn, S. P. Electronic Spectroscopy of Isoelectronic Molecules. II. Linear Triatomic Groupings Containing Sixteen Valence Electrons. *Chem. Rev.* **1971**, *71*, 73−108.

(18) Conroy, D.; Aristov, V.; Feng, L.; Sanov, A.; Reisler, H. Competitive Pathways via Nonadiabatic Transitions in Photodissociation. *Acc. Chem. Res.* **2001**, *34*, 625−632.

(19) Spiglanin, T. A.; Perry, R. A.; Chandler, D. W. Photodissociation Studies of HNCO: Heat of Formation and Product Branching Ratios. *J. Phys. Chem.* **1986**, *90*, 6184−6189.

(20) Yu, S. R.; Su, S.; Dorenkamp, Y.; Wodtke, A. M.; Dai, D. X.; Yuan, K. J.; Yang, X. M. Competition between Direct and Indirect Dissociation Pathways in Ultraviolet Photodissociation of HNCO. *J. Phys. Chem. A* **2013**, *117*, 11673−11678.

(21) Klossika, J. J.; Flothmann, H.; Beck, C.; Schinke, R.; Yamashita, K. The Topography of the HNCO(S_1) Potential Energy Surface and Its Implications for Photodissociation Dynamics. *Chem. Phys. Lett.* **1997**, *276*, 325−333.

(22) Brown, S. S.; Berghout, H. L.; Crim, F. F. Internal Energy Distribution of the NCO Fragment from Near-Threshold Photolysis of Isocyanic Acid, HNCO. *J. Phys. Chem.* **1996**, *100*, 7948−7955.

(23) Brown, S. S.; Metz, R. B.; Berghout, H. L.; Crim, F. F. Vibrationally Mediated Photodissociation of Isocyanic Acid (HNCO): Preferential N-H Bond Fission by Excitation of the Reaction Coordinate. *J. Chem. Phys.* **1996**, *105*, 6293−6303.

(24) Berghout, H. L.; Brown, S. S.; Delgado, R.; Fleming Crim, F. Nonadiabatic Effects in the Photodissociation of Vibrationally Excited HNCO: The Branching Between Singlet ($a^1\Delta$) and Triplet ($X^3\Sigma$-) NH. *J. Chem. Phys.* **1998**, *109*, 2257−2263.

(25) Brown, S. S.; Berghout, H. L.; Crim, F. F. The HNCO Heat of Formation and the N-H and C-N Bond Enthalpies from Initial State Selected Photodissociation. *J. Chem. Phys.* **1996**, *105*, 8103−8110.

(26) Zhang, J. S.; Dulligan, M.; Wittig, C. HNCO + $h\nu$(193.3 nm) → H + NCO: Center-of-Mass Translational Energy Distribution, Reaction Dynamics, and D_o(H-NCO). *J. Phys. Chem.* **1995**, *99*, 7446−7452.

(27) Yu, S. R.; Su, S.; Dai, D. X.; Yuan, K. J.; Yang, X. M. Vacuum Ultraviolet Photodissociation Dyanmics of Isocyanic Acid: The Hydrogen Elimination Channel. *J. Phys. Chem. A* **2013**, *117*, 13564−13571.

(28) Zyrianov, M.; Droz-Georget, T.; Reisler, H. Fragment Recoil Anisotropies in the Photoinitiated Decomposition of HNCO. *J. Chem. Phys.* **1999**, *110*, 2059−2068.

(29) Kaledin, A. L.; Cui, Q.; Heaven, M. C.; Morokuma, K. Ab Initio Theoretical Studies on Photodissociation of HNCO upon $S_1(^1A'')$←$S_0(^1A')$ Excitation: The Role of Internal Conversion and Intersystem Crossing. *J. Chem. Phys.* **1999**, *111*, 5004−5016.

(30) Droz-Georget, T.; Zyrianov, M.; Sanov, A.; Reisler, H. Photodissocation of HNCO: Three Competing Pathways. *Ber. Bunsen-Ges. Phys. Chem.* **1997**, *101*, 469−477.

(31) Droz-Georget, T.; Zyrianov, M.; Reisler, H.; Chandler, D. W. Correlated Distributions in the Photodissociation of HNCO to NH($X^1\Sigma$-, $a^1\Delta$)+CO($X^1\Sigma^+$) Near the Barrier on S_1. *Chem. Phys. Lett.* **1997**, *276*, 316−324.

(32) Klossika, J. J.; Schinke, R. The Photodissociation of HNCO in the S_1 Band: A Five-dimensional Classical Trajectory Study. *J. Chem. Phys.* **1999**, *111*, 5882−5896.

(33) Fujimoto, G. T.; Umstead, M. E.; Lin, M. C. Dynamics of CO Formation in the Photodissociation of HNCO and CH_2CO at 193 nm. *Chem. Phys.* **1982**, *65*, 197−203.

(34) Spiglanin, T. A.; Perry, R. A.; Chandler, D. W. Internal State Distributions of CO from HNCO Photodissociation. *J. Chem. Phys.* **1987**, *87*, 1568−1576.

(35) Spiglanin, T. A.; Chandler, D. W. Rotational State Distributions of NH($a^1\Delta$) from HNCO Photodissociation. *J. Chem. Phys.* **1987**, *87*, 1577−1581.

(36) Zyrianov, M.; Droz-Georget, T. H.; Sanov, A.; Reisler, H. Competitive Photodissociation Channels in Jet Cooled HNCO: Thermochemistry and Near-threshold Predissociation. *J. Chem. Phys.* **1996**, *105*, 8111−8116.

(37) Zyrianov, M.; Droz-Georget, T. H.; Reisler, H. Competition Between Singlet and Triplet Channels in the Photoinitiated Decomposition of HNCO. *J. Chem. Phys.* **1997**, *106*, 7454−7457.

(38) Wang, H.; Liu, S. L.; Liu, J.; Wang, F. Y.; Jiang, B.; Yang, X. M. Photofragment Imaging of HNCO Decomposition at 210 nm: The Primary NH($a^1\Delta$) + CO($X^1\Sigma^+$) Channel. *Chin. J. Chem. Phys.* **2007**, *20*, 388−394.

https://doi.org/10.1021/jacsau.3c00414
JACS Au 2023, 3, 2855−2861

(39) Zhang, Z. G.; Xin, M.; Zhao, S. T.; Chen, Y. Imaging Isocyanic Acid Photodissociation at 193 nm: The NH($a^1\Delta$) + CO($X^1\Sigma^+$) Channel. *Chin. J. Chem. Phys.* **2018**, *31*, 27−32.
(40) Zhang, Z. G.; Xin, M.; Wu, Y. N.; Zhao, S. T.; Tang, Y. J.; Chen, Y. Imaging HNCO Photodissociation at 201 nm: State-to-State Correlations between CO ($X^1\Sigma^+$) and NH ($a^1\Delta$). *Chin. J. Chem. Phys.* **2018**, *31*, 735−740.
(41) Zhang, Z. G.; Chen, Z. C.; Huang, C. S.; Chen, Y.; Dai, D. X.; Parker, D. H.; Yang, X. M. Imaging the Pair-correlated HNCO Photodissociation: The NH($a^1\Delta$) + CO($X^1\Sigma^+$) Channel. *J. Phys. Chem. A* **2014**, *118*, 2413−2418.
(42) Bonnet, L.; Linguerri, R.; Hochlaf, M.; Yazidi, O.; Halvick, P.; Francisco, J. S. Full-Dimensional Theory of Pair-Correlated HNCO Photofragmentation. *J. Phys. Chem. Lett.* **2017**, *8*, 2420−2424.
(43) Zhou, J.; Luo, Z.; Yang, J.; Chang, Y.; Zhang, Z.; Yu, Y.; Li, Q.; Cheng, G.; Chen, Z.; He, Z.; Che, L.; Yu, S.; Wu, G.; Yuan, K.; Yang, X. State-to-state Photodissociation Dynamics of CO_2 Around 108 nm: The O(^{1}S) Atom Channel. *Phys. Chem. Chem. Phys.* **2020**, *22*, 6260−6265.
(44) Zhang, Z.; Yang, S.; Li, Z.; Chang, Y.; Luo, Z.; Zhao, Y.; Yu, S.; Yuan, K.; Yang, X. Slice Imaging Study of NO_2 Photodissociation via the 1^2B_2 and 2^2B_2 States: The NO($X^2\Pi$)+O(^3P_J) Product Channel. *Phys. Chem. Chem. Phys.* **2023**, *25*, 16872−16880.
(45) Zhou, J. M.; Zhao, Y. R.; Hansen, C. S.; Yang, J. Y.; Chang, Y.; Yu, Y.; Cheng, G. K.; Chen, Z. C.; He, Z. G.; Yu, S. R.; Ding, H. B.; Zhang, W. Q.; Wu, G. R.; Dai, D. X.; Western, C. M.; Ashfold, M. N. R.; Yuan, K. J.; Yang, X. M. Ultraviolet Photolysis of H_2S and Its Implications for SH Radical Production in the Interstellar Medium. *Nat. Commun.* **2020**, *11*, 1547.
(46) Chang, Y.; An, F.; Chen, Z.; Luo, Z.; Zhao, Y.; Hu, X.; Yang, J.; Zhang, W.; Wu, G.; Xie, D.; Yuan, K.; Yang, X. Vibrationally Excited Molecular Hydrogen Production from the Water Photochemistry. *Nat. Commun.* **2021**, *12*, 6303.
(47) Chen, Z.; Shuai, Q.; Eppink, A. T. J. B.; Jiang, B.; Dai, D. X.; Yang, X. M.; Parker, D. H. Imaging CH_3SH Photodissociation at 204 nm: The SH + CH_3 Channel. *Phys. Chem. Chem. Phys.* **2011**, *13*, 8531−8536.
(48) Demyanenko, A. V.; Dribinski, V.; Reisler, H.; Meyer, H.; Qian, C. X. W. Product Quantum State Dependent Anisotropies in Photoinitiated Unimolecular Decomposition. *J. Chem. Phys.* **1999**, *111*, 7383−7396.
(49) Xie, Y.; Zhao, H.; Wang, Y.; Huang, Y.; Wang, T.; Xu, X.; Xiao, C.; Sun, Z.; Zhang, D. H.; Yang, X. Quantum Interference in H + HD → H_2 + D between Direct Abstraction and Roaming Insertion Pathways. *Science.* **2020**, *368*, 767−771.
(50) Han, S.; Zheng, X.; Ndengué, S.; Song, Y.; Dawes, R.; Xie, D.; Zhang, J.; Guo, H. Dynamical Interference in the Vibronic Bond Breaking Reaction of HCO. *Sci. Adv.* **2019**, *5*, No. eaau0582.
(51) Li, Z.; Zhao, M.; Xie, T.; Luo, Z.; Chang, Y.; Cheng, G.; Yang, J.; Chen, Z.; Zhang, W.; Wu, G.; Wang, X.; Yuan, K.; Yang, X. Direct Observation of the C + S_2 Channel in CS_2 Photodissociation. *J. Phys. Chem. Lett.* **2021**, *12*, 844−849.
(52) Zhao, Y.; Chen, J.; Luo, Z.; Li, Z.; Yang, S.; Chang, Y.; An, F.; Chen, Z.; Yang, J.; Wu, G.; Zhang, W.; Hu, X.; Xie, D.; Ding, H.; Yuan, K.; Yang, X. Photodissociation of H_2S: A New Pathway for the Production of Vibrationally Excited Molecular Hydrogen in the Interstellar Medium. *J. Phys. Chem. Lett.* **2022**, *13*, 9786−9792.
(53) Chang, Y.; Li, Q.; An, F.; Luo, Z.; Zhao, Y.; Yu, Y.; He, Z.; Chen, Z.; Che, L.; Ding, H.; Zhang, W.; Wu, G.; Hu, X.; Xie, D.; Plane, J. M. C.; Feng, W.; Western, C. M.; Ashfold, M. N. R.; Yuan, K. J.; Yang, X. M. Water Photolysis and Its Contributions to the Hydroxyl Dayglow Emissions in the Atmospheres of Earth and Mars. *J. Phys. Chem. Lett.* **2020**, *11*, 9086−9092.
(54) Chang, Y.; Ashfold, M. N. R.; Yuan, K. J.; Yang, X. M. Exploring the Vacuum Ultraviolet Photochemistry of Astrochemically Important Triatomic Molecules. *Nat. Sci. Rev.* **2023**, nwad158.
(55) Johnson III, R. D.; Hudgens, J. W. New Electronic States of NH and ND Observed from 258 to 288 nm by Resonance Enhanced Multipoton Ionization Spectroscopy. *J. Chem. Phys.* **1990**, *92*, 6420−6425.
(56) Fu, B.; Zhang, D. H. Ab Initio Potential Energy Surfaces and Quantum Dynamics for Polyatomic Bimolecular Reactions. *J. Chem. Theory Comput.* **2018**, *14*, 2289−2303.
(57) Lu, X.; Shang, C.; Li, L.; Chen, R.; Fu, B.; Xu, X.; Zhang, D. H. Unexpected Steric Hindrance Failure in the Gas Phase F- + $(CH_3)_3CI$ S_N2 Reaction. *Nat. Commun.* **2022**, *13*, 4427.
(58) Chen, R.; Shao, K.; Fu, B.; Zhang, D. H. Fitting Potential Energy Surfaces with Fundamental Invariant Neural Network. II. Generating Fundamental Invariants for Molecular Systems with up to Ten Atoms. *J. Chem. Phys.* **2020**, *152*, 204307.
(59) Shao, K.; Chen, J.; Zhao, Z.; Zhang, D. H. Communication: Fitting Potential Energy Surfaces with Fundamental Invariant Neural Network. *J. Chem. Phys.* **2016**, *145*, 071101.
(60) Schinke, R. *Photodissociation dynamics: spectroscopy and fragmentation of small polyatomic molecules*; Cambridge University Press: 1995.
(61) Fu, B.; Shepler, B. C.; Bowman, J. M. Three-state Trajectory Surface Hopping Studies of the Photodissociation Dynamics of Formaldehyde on Ab Initio Potential Energy Surfaces. *J. Am. Chem. Soc.* **2011**, *133*, 7957−7968.
(62) Bonnet, L. Classical Dynamics of Chemical Reactions in a Quantum Spirit. *Int. Rev. Phys. Chem.* **2013**, *32*, 171−228.
(63) Gutzwiller, M. C. *Chaos in classical and quantum mechanics*; Springer Science & Business Media, 2013; Vol. *1*.

https://doi.org/10.1021/jacsau.3c00414
JACS Au 2023, 3, 2855−2861